Radiomic Analysis of the Heterogeneous Tumor and Surrounding Parenchyma Based on DCE-MRI Decomposition to Predict HER2 Expression in Breast Cancer

Peng Zhang
School of Biological Science and Medical Engineering, Beihang University, Beijing 100191, China
Juan Yan
China CDC Key Laboratory of Radiological Protection and Nuclear Emergency, National Institute for Radiological Protection, Chinese Center for Disease Control and Prevention, Beijing 100088, China
Zhongqi Liu
School of Biological Science and Medical Engineering, Beihang University, Beijing 100191, China
Xiangsheng Li
Department of Magnetic Resonance Imaging, Air Force Medical Center of PLA, Beijing 100142, China
Qianxiang Zhou (zhouqianxiangbme@163.com)
Beihang University https://orcid.org/0000-0002-6235-2840

Research article

Keywords: Breast cancer, HER2 expression, DCE-MRI, Decomposition, Predictor

Posted Date: July 7th, 2021

DOI: https://doi.org/10.21203/rs.3.rs-638341/v1

Abstract

Background Human epidermal growth factor receptor-2 (HER2) correlates with cancer heterogeneity, and the identification of HER2 expression is invasive immunohistochemistry in the clinic. To determine whether noninvasive predictors of HER2 expression are implied in the dynamic contrast-enhanced magnetic resonance imaging (DCE-MRI).

Methods 189/47 breast cancer patients collected from The Cancer Imaging Archive (TCIA) were used as a cross-validation/test group. A convex analysis of mixtures (CAM) was conducted to decompose heterogeneous tissues inside and outside the tumor. Their DCE-MRI images were decomposed into relatively homogeneous subregions with different contrast enhancement patterns. The predictor of HER2 expression was composed of radiomic features acquired from intratumoural or peritumoural subregions. The area under the curve (AUC) of receiver operating characteristic (ROC) was used to assess the predictive power.

Results The predictor formed in the undecomposed tumor was used as a baseline for comparison (AUC=0.691±0.072/0.625±0.056 in cross-validation/test group). The intratumoural subregion with a contrast enhancement pattern corresponding to the plateau of signal intensity formed a more robust predictor (AUC=0.816±0.059/0.785±0.067, P=0.0128/0.0389). Peritumoral parenchyma of <20 mm from the tumor margin was also researched (AUC=0.589±0.083/0.524±0.064). The peritumoural subregion with a contrast enhancement pattern corresponding to steady enhancement also formed a helpful predictor compared to the undecomposed parenchyma (AUC=0.702±0.068/0.681±0.042, P=0.0128/0.0389). The best predictor was formed when two predictors from subregions were fused together (AUC=0.851±0.057/0.812±0.045, P=0.0011/0.0397).

Conclusions A subregion rather than a heterogeneous tumor itself provided a more accurate predictor of HER2 expression. Radiomic predictors from intratumoural and peritumoural subregions were complementary to each other.

Introduction

Human epidermal growth factor receptor-2 (HER2) is over-expressed in 20–25% of breast cancers. HER2- targeted therapy is an effective treatment for patients [1, 2]. Clinical trials have shown that patients of metastatic HER2-positive have significantly longer progression-free survival after first-line therapy with *pertuzumab* than in those treated with placebo [3]. HER2 is also a critical prognostic factor of breast cancer. Patients tend to show a worse prognosis when the HER2 expression is positive [4, 5]. Although HER2 is essential for treatment and significant for prognosis, the identification of HER2 expression is invasive immunohistochemistry in the clinic.

Dynamic contrast-enhanced magnetic resonance imaging (DCE-MRI) has been widely applied as a noninvasive method for diagnosing breast cancers. A previous study [6] has shown that radiomic features extracted from DCE-MRI associate with gene signatures used for evaluating prognosis. Researchers concentrating on radiology [7, 8] have already attempted to predict molecular subtypes, including HER2 expression, but malignant tumors consisting of subclones with various genetic alterations and functional roles are always heterogeneous [9, 10]. Thus, these radiological methods may have poor robustness in predicting HER2 expression. A recent study [11] focusing on multiscale intratumoural heterogeneity has reported that using radiomic features can classify patients with distinct subclone compositions. Thus the tumor heterogeneity needs to be analyzed for exacter research on breast cancers.

Tumor in the growth process is dynamically regulated by the surrounding microenvironment [12], and there is also continuous interaction between tech other [13, 14]. Unlike the intratumour tissues, peritumoural parenchyma, including the microenvironment, is genetically stable. Thus it can be used as a therapeutic target to reduce cancer recurrence and resistance risk [15, 16]. The background parenchymal enhancement is more clearly reflected on DCE-MRI, which can be used to research pathological mechanisms [17, 18]. A preliminary study [19] has reported that the background parenchymal enhancement around a tumor is associated with HER2 expression.

Physiological changes of intratumoural or peritumoural angiogenesis can be sensitively showed on DCE-MRI. Diverse voxels in DCE-MRI have different tracer kinetics that can reflect underlying tissue heterogeneity [20, 21]. Many studies had used original

[22–26] or clustered [27–29] DCE-MRI to reveal the correlation between heterogeneity and pathological expression. Owing to the partial volume effect (PVE) that tracer concentrations at many voxels often represent the mixture of more than one compartment, these studies using original or clustered DCE-MRI may be biased. PVE can lead to an incorrect estimation of the contrast enhancement pattern in heterogeneous tissues. A convex analysis of mixtures (CAM) can decompose DCE-MRI images into overlapping subregions so that PVE is effectively relieved [30, 31]. Despite the improvement of CAM in imaging decomposition, whether radiomic features from these subregions are better for predicting HER2 expression remains unclear.

In this study (Fig. 1), CAM decomposed heterogeneous tumor and surrounding parenchyma tissues into relatively homogeneous subregions with differential contrast enhancement patterns. The visual evaluation for a contrast enhancement pattern was focused on the shape of the time-signal intensity curve. For example, whether the signal intensity continued to increase after the initial upstroke (slow-flow), it was cut off and reached a plateau (fast-flow) or it washed out (plasma-input). The predictor of HER2 expression was built using radiomic features from an intratumoural or peritumoural subregion. We aimed to refine prediction accuracy based on the mutual complementation between a tumor and surrounding parenchyma.

Methods

Patient Selection

A retrospective study about breast cancer patients who had DCE-MRI and immunohistochemistry examinations simultaneously: two anonymized and published datasets were downloaded from The Cancer Imaging Archive (TCIA). The first dataset, including 222 female patients, was used as a cross-validation group, and the second dataset, including 64 female patients, was used as a test group (Fig.1a). Some overlapped patients were researched to predict recurrence-free survival after neoadjuvant chemotherapy in previous studies [32]. In the present study, patients (n=21) who had incomplete immunohistochemistry information of HER2 expression were excluded. Patients (n=24) who had incomplete DCE-MRI series were also excluded. There were also some patients (n=5) whose tumors could not be clearly observed on images. In the end, 189 patients in the cross-validation group and 47 patients in the test group met the research criteria.

MRI Acquisition

DCE-MRI of the cross-validation group was performed with a 1.5T system (Siemens Healthcare, Erlangen, Germany/General Electric Healthcare, Fairfield, America) by using a dedicated radiofrequency coil. The image acquisition protocol included a localization scan and T2-weighted sequence followed by a contrast-enhanced T1-weighted series. All imaging was performed unilaterally over the symptomatic breast and in the sagittal orientation. The contrast-enhanced series consisted of a high resolution (≤1mm in-plane spatial resolution) three-dimensional, fat-suppressed, T1-weighted gradient-echo sequence with TR≤20 ms, TE = 4.5 ms, flip angle ≤ 45º, 16-18 cm field-of-view, minimum matrix 256 192, 64 slices, slice thickness ≤ 2.5 mm. Scan time length for the T1-weighted sequence was required to be between 4.5 and 5 minutes. The sequence was acquired once before contrast injection and repeated at least twice following injection.

DCE-MRI of the test group was acquired on a 1.5-T scanner (General Electric Healthcare, Fairfield, America) by using a bilateral phased array coil. The imaging protocol included a 3D localizer and a unilateral sagittal DCE acquisition (TR/TE 8/4.2; flip angle 20 degrees; field of view 18-20 cm; acquisition matrix 256 192 60, section thickness 2 mm; spatial resolution 0.7 0.94 2.0 mm3). Imaging time was approximately 5 minutes per acquisition, resulting in effective early and late post-contrast time points of 2.5 minutes and 7.5 minutes from the start of the contrast injection, respectively, using standard k-space sampling. In addition, fat suppression was performed using a frequency-selective inversion recovery preparatory pulse.

Imaging Segmentation

The central position of each tumor was marked by an experienced radiologist who was blinded to any clinical or immunohistochemistry information. Image segmentation using a fuzzy C-means algorithm (FCM) [28] was performed on median postcontrast series. Skin and fatty tissues were excluded from breast images to get the entire parenchyma surrounding a tumor. Similar to the previous study [33], peritumoral parenchyma tissue of <20 mm from the tumor margin was researched.

The tissue boundary of each tumor or parenchyma was automatically produced by using a segmentation program on MATLAB v.2019a. These poor segmentations checked by our investigators were manually corrected.

DCE-MRI Decomposition

CAM decomposition tool (MATLAB source code can be downloaded at the website www.cbil.ece.vt.edu/software.htm) has been developed to dissect complex tissues into subregions with differential contrast enhancement patterns. Tracer concentration $x(i,t)$ of a voxel can be expressed as a nonnegative linear combination of latent tissue-specific compartmental time-series curves $a_j(t)$ and relative tissue type proportions $K_j(i)$, i.e., $x(i,t) = a_{t1}(t)K_1(i) + \cdots + a_j(t)K_j(i) + \cdots + a_J(t)K_J(i)$. DCE-MRI measured values satisfy the definition of a convex set [30, 31]:

$$\mathcal{X}_{\text{measured}} = \left\{ \sum_{j=1}^{J} K_j(i)\boldsymbol{a}_j \,\middle|\, K_j(i) \geq 0, \sum_{j=1}^{J} K_j(i) = 1, \ldots, N \right\}$$

j is the number of functional tissue compartments, and a_j is the vector notation of $a_j(t)$ over time.

There were different imaging protocols in patients between the cross-validation group and test group, so time intervals of the DCE-MRI series were different. Therefore, images between two slices were interpolated linearly to obtain a unified 60s time interval in this study. According to the definition in previous studies of CAM, three main subregions were termed slow-flow (steady enhancement), fast-flow (plateau of signal intensity), and plasma-input (washout of signal intensity), respectively. In addition, $K(i)$ of approximately one was defined as the pure subregion, and the $K(i)$ between zero to one was defined as the overlapped subregion (Fig.2).

Radiomic Features Extraction

Three-dimensional radiomic features, including texture and histogram, were valuable for signal intensity variation in DCE-MRI. Radiomic features have been widely used to quantify pathology characteristics in medical studies [23, 24, 27, 33]. As shown in Table 1, 18 texture features and ten histogram features were acquired from each DCE-MRI series. Signal intensities of DCE-MRI were changed along with imaging time after injecting tracer so that precontrast, median postcontrast, and last postcontrast series were utilized to acquire these radiomic features. In the end, 84 (18 3+10 3) features were extracted from images of an undecomposed tissue or a CAM subregion.

Statistical Analysis

The differences of patient race and tumor laterality were assessed using the X^2 test or Fisher's exact test if the expected frequency in any cell of the contingency table was <5. The differences in patient age, maximum diameter, lesion volume, and parenchymal density were assessed using analysis of variance (ANOVA). One-way ANOVA evaluated the variety of one feature between cancers with different HER2 expression, and the ability to predict HER2 expression was evaluated using a univariate logistic model. The random forest model formed by 84 radiomic features was built as the predictor of HER2 expression. The model was trained and tested using the leave-one-out cross-validation (LOOCV) method. The predictive power was assessed using the area under the curve (AUC) of receiver operating characteristic (ROC). In each LOOCV loop, a 10-fold cross-validation test was applied in the training set to achieve optimum parameters of the random forest model [34]. The 95% confidence interval of a single AUC and the comparison between two AUCs were determined using a bootstrap test. A two-tailed P of <0.05 was considered statistically significant, and Bonferroni correction was performed in multiple-comparison tests. All statistical analyses were performed on R v.3.4.2 and MATLAB v.2019a.

Results

Patient Characteristics

Table 2 summarizes the patient demographics and breast lesion characteristics. The mean age of 134(70.9%)/32(68.1%) HER2-negative patients was 47.9±9.0/47.9±10.1 years, and the mean age of 55(29.1%)/15(31.9%) HER2-positive patients was 47.8±8.8/45.3±8.7 years in the cross-validation/test group. The statistical results of patient race, laterality, age, maximum diameter, lesion volume, and parenchymal density were no significant differences between the HER2-positive and HER2-negative cancers. However, a statistically significant difference (P<0.0001, Fig.3a) was observed concerning the percentages of pure slow-flow subregions, which had relatively higher percentages inside HER2-negative tumors. In addition, the percentage of peritumoural slow-flow subregion was higher than that of fast-flow or plasma-input subregion.

The Outstanding Features in CAM Subregions

The predictive power of one single radiomic feature was assessed by one-way ANOVA and univariate logistic regression (Fig.4). In the undecomposed tumor/parenchyma, there was only one/no outstanding feature (The corrected P of the one-way ANOVA was <0.05, and the AUC of univariate logistic regression was >0.5). In pure fast-flow of the tumor/pure slow-flow subregion of the parenchyma, there were 18/6 outstanding features. Some radiomic features acquired from subregions got the lower P in one-way ANOVA and the higher AUC in univariate logistic regression. The most outstanding feature in intratumoural subregions was the entropy acquired from the median postcontrast series (The corrected P was 0.0012 and the AUC was 0.601). The most outstanding feature in peritumoural subregions was the sum variance acquired from the last postcontrast series (The corrected P was 0.0078 and the AUC was 0.584).

The Predictors Formed by Radiomic Features in CAM Subregions

The predictor formed by 84 radiomic features in each region was built to predict HER2 expression. The predictive result was evaluated to explore the association of an undecomposed region or CAM subregion with HER2 expression. As shown in Table 3, the predictor formed in undecomposed tumors got an AUC of 0.691±0.072/0.625±0.056 in the cross-validation/test group. AUC was increased to 0.816±0.059/0.785±0.067 (P was 0.0128/0.0389) when the predictor was formed by radiomic features acquired from intratumoural pure fast-flow subregion. The predictor formed in undecomposed parenchyma got an AUC of 0.589±0.083/0.524±0.064. AUC was increased to 0.702±0.068/0.681±0.042 (P was 0.0204/0.0407) when the predictor was formed by radiomic features acquired from the peritumoural pure slow-flow subregion.

The Fusion of Intratumoural and Peritumoural Predictor

The best intratumoural and peritumoural predictors were fused to take respective advantages for predicting HER2 expression (Fig.5). The predictive fusion value of a testing sample was a weighted summation of two predictive values from the best intratumoural and peritumoural predictor. The weight coefficients of this weighted summation were two AUCs obtained in training samples. Comparing with the predictor formed in the undecomposed tumor, AUC was higher after fusing predictors formed in undecomposed tumor and parenchyma (AUC was 0.716/0.647, P was 0.7525/0.8696 in cross-validation/test group). However, AUC was increased more evidently when the best intratumoural and peritumoural predictors were fused (AUC was 0.851/0.812, P was 0.0011/0.0397).

The Comparison of Fusion Predictors

In this study, the tumor and parenchyma were partitioned into subregions using kinetic pattern clustering (KPC), time to peak (TTP), or peak enhancement rate (PER) method [28]. Their best predictors formed in the intratumoural and peritumoural subregion were also fused to compare with the fusion predictor formed by the undecomposed tumor and parenchyma (UTP) method. These ROCs are shown in Fig.5. Comparing with the fusion predictor formed by the UTP method (Table 4), AUC was higher after fusing the best intratumoural and peritumoural predictor formed by KPC, TTP, PER, or CAM. However, only the AUC of the fusion predictor formed by the CAM method significantly differed (P was 0.0099/0.0450 in the cross-validation/test group).

Discussion

Breast cancer heterogeneity of contrast enhancement patterns on DCE-MRI can be discovered by decomposition using CAM. Patient characteristics including race, laterality, age, maximum diameter, lesion volume, and parenchymal density were no significant differences between HER2-positive and HER2-negative cancers, but contrast enhancement patterns of a tumor were heterogeneous. The tracer concentrations of DCE-MRI often represent a mixture of more than one distinct compartment owing to PVE. If the DCE-MRI is not decomposed into subregions using CAM, breast cancer heterogeneity of contrast enhancement patterns cannot be discovered. The pure slow-flow subregions had a steady enhancement shape of tracer concentrations, higher inside HER2-negative tumors (P<0.0001). HER2-positive cancer exhibits a stronger tendency toward malignant growth characteristics [35]. A higher percentage of pure slow-flow subregion implies that HER2-negative cancer has more components akin to benign lesions. Although the parenchymal densities around tumors were not significantly different (ANOVA, P=0.3914), the peritumoural contrast enhancement pattern of steady enhancement had a higher proportion.

Radiomic features acquired from CAM subregions were more helpful in predicting HER2 expression than those from undecomposed regions. One-way ANOVA and univariate logistic results proved that more outstanding radiomic features were in CAM subregions. Only one outstanding feature was in the undecomposed tumor, but the number of outstanding features increased to 18 in the pure fast-flow subregion. This phenomenon implied that the intratumoural subregion with contrast enhancement pattern corresponding to the plateau of the signal intensity provided more valuable features for predicting HER2 expression. Although no outstanding feature was in the undecomposed parenchyma, six outstanding features were discovered in the peritumoural pure slow-flow subregion. This phenomenon implied that the peritumoural subregion with contrast enhancement pattern corresponding to the steady enhancement helped predict HER2 expression.

Intratumoural pure fast-flow subregion with contrast enhancement pattern corresponding to the plateau of signal intensity had a more robust predictor for HER2 expression. Previous studies [22-26, 28, 29] using DCE-MRI have demonstrated the correlation of kinetic heterogeneity with clinical characteristics or molecular subtypes. However, these were possibly imperfect owing to multiple contrast enhancement patterns inside a tumor. This study was also based on the observation that the analysis of kinetic heterogeneity on DCE-MRI was necessary, but the CAM method was conducted to decompose images into subregions. The predictor based on radiomic features from the undecomposed tumor got an AUC of 0.691±0.072/0.625±0.056 in the cross-validation/test group, and the AUC increased to 0.816±0.059/0.785±0.067 with a P of 0.0128/0.0389 when the predictor was established using the radiomic features from intratumoural the pure fast-flow subregion.

Peritumoural pure slow-flow subregion with contrast enhancement pattern corresponding to the steady enhancement also provided a helpful predictor for HER2 expression. Peritumoural parenchyma, including the microenvironment, is genetically stable, unlike the tumor, but it can regulate cancer development dynamically. A preliminary study [19] reported that HER2 expression is associated with background parenchymal enhancement. Thus, the tumor and the surrounding parenchyma (peritumoral parenchyma tissue of <20 mm from the tumor margin) were decomposed into subregions using CAM in this study. The predictor based on radiomic features acquired from the undecomposed parenchyma got an AUC of 0.589±0.083/0.524±0.064 in the cross-validation/test group, and the AUC increased to 0.702±0.068/0.681±0.042 with a P of 0.0204/0.0407 when the predictor was established using the radiomic features from peritumoural pure slow-flow subregion.

Intratumoural and peritumoural predictors complemented each other, and the best predictor was formed when two predictors were fused. Previous studies [12-14] have demonstrated that the microenvironment dynamically regulates heterogeneous tumors, and the interaction between tumor and surrounding microenvironment is continuous. However, whether peritumoural tissues can develop the predictor of HER2 expression remains unclear. In our experiments, when two predictors from the intratumoural and peritumoural subregion were fused, the AUC increased to 0.851±0.057/0.812±0.045 from 0.816±0.059/0.785±0.067 in the cross-validation/test group. This result indicates that the peritumoural subregion can improve prediction accuracy, although it cannot predict HER2 expression accurately.

CAM is a more effective method to define the subregions correlating with HER2 expression than others. The predictive performance of radiomic features was improved by clustering DCE-MRI based on KPC, TTP, or PER [28], but whether CAM decomposition of DCE-MRI was more helpful in predicting HER2 expression was not researched. The best intratumoural predictor was from the pure fast-flow subregion, and the best peritumoural predictor was from the pure slow-flow subregion.

The two best predictors were formed in pure subregion rather than overlapped subregion, implying that if a subregion correlating to HER2 expression was pure, the correlation was stronger. However, clustering methods, including KPC, TTP, and PER, have not defined the pure subregion. The AUC was 0.716±0.051/0.647±0.043 when two predictors from intratumoural and peritumoural undecomposed tissues were fused, which increased to 0.757±0.063/0.708±0.052 with P=0.5161/0.6362 using KPC, 0.792±0.069/0.734±0.047 with P=0.1410/0.4812 using TTP, 0.771±0.054/0.729±0.043 with P=0.3099/0.4654 using PER, or 0.851±0.057/0.812±0.045 with P=0.0099/0.0450 using CAM. This result demonstrated that clustering DCE-MRI by KPC, TTP, or PER could improve the predictive ability for HER2 expression, but it was worse than decomposing DCE-MRI by CAM.

There was a preliminary study for predicting the HER2 expression of breast cancer based on DCE-MRI decomposition, and several limitations should be considered when interpreting the results: 1. It would be valuable to perform heterogeneity analysis based on other radiological technology, such as DW-MRI and molybdenum target imaging, to validate and extend this work. 2. The statistical results are likely to have been affected by selection bias because of the limited number of samples and single-center scope. If there is an inclusion of datasets from different medical institutions would provide more valid results. 3. We focused on a priori analyses of parenchyma that were <20 mm from the tumor margin and ignored individual differences in breast tissues.

Conclusions

In conclusion, intratumoural and peritumoural subregions based on DCE-MRI decomposition can improve the prediction of HER2 expression using radiomic features. These findings potentially have clinical benefits because they would identify the HER2 expression of patients for individualized therapies without intrusive biopsy checks. However, a lot of research work is needed before this method can be utilized in clinical practice.

Abbreviations

CAM	convex analysis of mixtures	PVE	partial volume effect
FCM	fuzzy C-means algorithm	TIC	time-signal intensity curves
AUC	area under the curve	KPC	kinetic pattern clustering
PER	peak enhancement rate	TTP	time to peak
LOOCV	leave-one-out cross validation	UTP	undecomposed tumor and parenchyma

Declarations

Ethical Approval and Consent to Participate There is a retrospective study. Two anonymized and published datasets were downloaded from The Cancer Imaging Archive (TCIA). TCIA is a public data set, so the Ethical Approval and Consent to Participate are not applicable.

Consent for Publication The consent for publication was obtained from all participants.

Availability of Supporting Data The dataset of cross-validation group is available from ISPY1 of TCIA [https://wiki.cancerimagingarchive.net/display/Public/ISPY1]. The dataset of test group is available from Breast-MRI-NACT-Pilot of TCIA [https://wiki.cancerimagingarchive.net/display/Public/Breast-MRI-NACT-Pilot].

Code Availability Codes for convex analysis of mixtures (CAM) are available on the website [www.cbil.ece.vt.edu/software.htm].

Competing Interests The authors declare no conflict of interest.

Funding This study was funded by the CDC of China, grant number C20190736.

Author contributions P.Z. and Q.Z. Designed the study, finished the experiments, and wrote the paper. P.Z. and J.Y. contributed to the study design, image processing, and statistical analysis. Z.L. participated was a significant contributor in reviewing and editing the paper. X.L. participated in the clinical analysis and contributed to marking the lesion. All authors read and approved the final paper.

Acknowledgments The authors thank David Newitt, Ph.D., and Nola Hylton, Ph.D. from the Breast Imaging Research Program at the University of California, San Francisco (UCSF), for providing shared data on The Cancer Imaging Archive (TCIA).

References

1. Lehmann BD, Bauer JA, Chen X, Sanders ME, Chakravarthy AB, Shyr Y, Pietenpol JA. Identification of human triple-negative breast cancer subtypes and preclinical models for selection of targeted therapies. The Journal of Clinical Investigation. 2011; 121(7):2750-2767.
2. Duso B, Poletti C, Curigliano G, Pelicci P, Mazzarella L. Secondary mechanisms of anti-HER2 resistance in breast cancer: NF1 as an actionable target. Ann Oncol. 2019; 30(Supplement 3):iii6-iii7.
3. Swain SM, Baselga J, Kim S-B, Ro J, Semiglazov V, Campone M, Ciruelos E, Ferrero J-M, Schneeweiss A, Heeson S *et al*. Pertuzumab, trastuzumab, and docetaxel in HER2-positive metastatic breast cancer. N Engl J Medicine. 2015; 372(8):724-734.
4. Ménard S, Balsari A, Tagliabue E, Camerini T, Casalini P, Bufalino R, Castiglioni F, Carcangiu ML, Gloghini A, Scalone S *et al*. Biology, prognosis and response to therapy of breast carcinomas according to HER2 score. Ann Oncol. 2008; 19(10):1706-1712.
5. Li H, Zhu Y, Burnside ES, Huang E, Drukker K, Hoadley KA, Fan C, Conzen SD, Zuley M, Net JM *et al*. Quantitative MRI radiomics in the prediction of molecular classifications of breast cancer subtypes in the TCGA/TCIA data set. NPJ Breast Cancer. 2016; 2:16012.
6. Van der Velden B, Schmitz AMT, Loo C, Gilhuijs KGA. Association between computer-derived features of the ipsilateral breast on DCE-MRI and the 70-gene signature in patients with invasive breast cancer. Cancer Res. 2016; 76(4):P4-02-07.
7. Fan M, Yuan W, Zhao WR, Xu MS, Li LH. Joint prediction of breast cancer histological grade and Ki-67 expression level based on DCE-MRI and DWI radiomics. IEEE Journal of Biomedical and Health Informatics. 2019; 24(6):1632-1642.
8. Zhang Y, Chen J-H, Lin Y, Chan S, Zhou J, Chow D, Chang P, Kwong T, Yeh D-C, Wang X *et al*. Prediction of breast cancer molecular subtypes on DCE-MRI using convolutional neural network with transfer learning between two centers. Eur Radiol. 2021; 31(4):2559-2567.
9. Scaling A, Knox A, Pinto M, Bliesner B, Haughian J, Abdel-Hafiz H, Horwitz K. Abstract P2-04-05: Modeling luminal breast cancer heterogeneity: Combination therapies to suppress hormone receptor-negative subpopulations among receptor-positive ones. Cancer Res. 2015; 75(9):P2-04-05.
10. Zardavas D, Irrthum A, Swanton C, Piccart M. Clinical management of breast cancer heterogeneity. Nature Reviews Clinical Oncology. 2015; 12(7):381-394.
11. Fan M, Xia P, Clarke R, Wang Y, Li L. Radiogenomic signatures reveal multiscale intratumour heterogeneity associated with biological functions and survival in breast cancer. Nature Communications. 2020; 11(1):4861-4872.
12. Tlsty TD, Coussens LM. Tumor stroma and regulation of cancer development. Annu Rev Pathol. 2006; 1:119-150.
13. Mao Y, Keller ET, Garfield DH, Shen K, Wang J. Stromal cells in tumor microenvironment and breast cancer. Cancer Metastasis Reviews. 2013; 32(1-2):303-315.
14. Hanahan D, Coussens LM. Accessories to the crime: functions of cells recruited to the tumor microenvironment. Cancer Cell. 2012; 21(3):309-322.
15. Quail DF, Joyce JA. Microenvironmental regulation of tumor progression and metastasis. Nat Med. 2013; 19(11):1423-1437.

16. Monsky WL, Mouta Carreira C, Tsuzuki Y, Gohongi T, Fukumura D, Jain RK. Role of host microenvironment in angiogenesis and microvascular functions in human breast cancer xenografts: mammary fat pad versus cranial tumors. Clin Cancer Res. 2002; 8(4):1008-1013.
17. Thompson CM, Mallawaarachchi I, Dwivedi DK, Ayyappan AP, Dwivedi AK. The association of background parenchymal enhancement at breast MRI with breast cancer: a systematic review and meta-analysis. Radiology. 2019; 292(3):1-10.
18. Kim S-A, Cho N, Ryu EB, Seo M, Bae MS, Chang JM, Moon WK. Background parenchymal signal enhancement ratio at preoperative MR imaging: association with subsequent local recurrence in patients with ductal carcinoma in situ after breast conservation surgery. Radiology. 2014; 270(3):699-707.
19. Wu S, Zuley ML, Kurland BF, Jankowitz RC, Gur D. Abstract P1-01-06: Quantitative breast DCE-MRI risk biomarkers and breast tumor immunohistochemistry phenotypes: A preliminary assessment. Cancer Res. 2015; 75(Supplement 9):10.1158/1538-7445.
20. Mahrooghy M, Ashraf AB, Daye D, Mcdonald ES, Rosen M, Mies C, Feldman M, Kontos D. Pharmacokinetic tumor heterogeneity as a prognostic biomarker for classifying breast cancer recurrence risk. IEEE Trans Biomed Eng. 2015; 62(6):1585-1594.
21. Wang N, Gong T, Clarke R, Chen L, Shih IM, Zhang Z, Levine DA, Xuan J, Wang Y. UNDO: a Bioconductor R package for unsupervised deconvolution of mixed gene expressions in tumor samples. Bioinformatics. 2015; 31(1):137-139.
22. Syed A, Sorace AG, Barnes SL, Arlinghaus L, Xia L, Yankeelov TE. Abstract 3941: Assessing heterogeneity in DCE-MRI data of breast cancer to predict treatment response. Cancer Res. 2017; 77(Supplement 13):3941-3941.
23. Kim JH, Ko ES, Lim Y, Lee KS, Han BK, Ko EY, Hahn SY, Nam SJ. Breast cancer heterogeneity: MR imaging texture analysis and survival outcomes. Radiology. 2016; 282(3):665-675.
24. Agner SC, Rosen MA, Englander S, Tomaszewski JE, Feldman MD, Zhang P, Mies C, Schnall MD, Madabhushi A. Computerized image analysis for identifying triple-negative breast cancers and differentiating them from other molecular subtypes of breast cancer on dynamic contrast-enhanced MR images: a feasibility study. Radiology. 2014; 272(1):91-99.
25. Chitalia R, Rowland J, McDonald E, Pantalone L, Cohen E, Gastounioti A, Feldman M, Schnall M, Conant E, Kontos D. Imaging phenotypes of breast cancer heterogeneity in preoperative breast dynamic contrast enhanced magnetic resonance imaging (DCE-MRI) scans predict 10-Year recurrence. Clin Cancer Res. 2020; 26(4):862-869.
26. Mazurowski MA, Zhang J, Grimm LJ, Yoon SC, Silber JI. Radiogenomic analysis of breast cancer: luminal B molecular subtype is associated with enhancement dynamics at MR imaging. Radiology. 2014; 273(2):365-372.
27. Longo DL, Dastrù W, Consolino L, Espak M, Arigoni M, Cavallo F, Aime S. Cluster analysis of quantitative parametric maps from DCE-MRI: application in evaluating heterogeneity of tumor response to antiangiogenic treatment. Magn Reson Imaging. 2015; 33(6):725-736.
28. Fan M, Cheng H, Zhang P, Gao X, Zhang J, Shao GL, Li LH. DCE-MRI texture analysis with tumor subregion partitioning for predicting Ki-67 status of estrogen receptor-positive breast cancers. JMagnResonImaging. 2017.
29. You KJ, Joo KJ, Lee H, Bum SH, Suk K, Seok CK, Jin NK, Taewoo K. Kinetic heterogeneity of breast cancer determined using computer-aided diagnosis of preoperative MRI scans: relationship to distant metastasis-free survival. Radiology. 2020; 295(3):517-526.
30. Li C, Chan T-H, Choyke PL, Hillman EMC, Chi C-Y, Bhujwalla ZM, Wang G, Wang SS, Szabo Z, Wang Y. CAM-CM: a signal deconvolution tool for in vivo dynamic contrast-enhanced imaging of complex tissues. Bioinformatics. 2011; 27(18):2607-2615.
31. Li C, Choyke PL, Chan TH, Chi CY, Wang G, Wang Y. Tissue-Specific Compartmental Analysis for Dynamic Contrast-Enhanced MR Imaging of Complex Tumors. IEEE Trans Med Imaging. 2011; 30(12):2044-2058.
32. Hylton NM, Gatsonis CA, Rosen MA, Lehman CD, Schnall MD. Neoadjuvant chemotherapy for breast cancer: functional tumor volume by MR imaging predicts recurrence-free survival-results from the ACRIN 6657/CALGB 150007 I-SPY 1 TRIAL. Radiology. 2016; 279(1):44-55.
33. Wu J, Li BL, Sun XL, Cao GH, Rubin DL, Napel S, Ikeda DM, Kurian AW, Li RJ. Heterogeneous enhancement patterns of tumor-adjacent parenchyma at MR imaging are associated with dysregulated signaling pathways and poor survival in

breast cancer. Radiology. 2017; 285(2):401-413.
34. Huynh T, Gao Y, Kang J, Wang L, Zhang P, Lian J, Shen D. Estimating CT image from MRI data using structured random forest and auto-context model. IEEE Trans Med Imaging. 2015; 35(1):174-183.
35. Uematsu T, Kasami M, Yuen S. Triple-Negative breast cancer: correlation between MR Imaging and pathologic findings. Radiology. 2009; 250(3):638-647.

Tables

Table 1 Summary of extracted radiomic features and description

Radiomic Features	Description
Autocorrelation [a]	Measures the magnitude of the fineness and coarseness of texture
Cluster Prominence [a]	Measures the skewness and asymmetry of the GLCM
Cluster Shade [a]	Measures the skewness and uniformity of the GLCM
Correlation [a]	Shows the linear dependency of gray-level values in the GLCM
Contrast [a]	Measures the local intensity variation presented in an image
Difference Entropy [a]	Randomness of the difference of neighboring voxel gray levels
Dissimilarity [a]	Shows the local contrasts
Difference Variance [a]	Variations of difference of gray-level pairs
Entropy [a]	Indicates the uncertainty of the GLCM
Energy [a]	A measure of the homogeneity of an image
Homogeneity [a]	A measure of local homogeneity
Inverse difference [a]	Another measure of the local homogeneity of an image
Information correlation 1 [a]	Nonlinear gray-level dependence
Information correlation 2 [a]	Another nonlinear gray-level dependence
Maximum probability [a]	Highest frequency of pixel pair
Sum average [a]	Shows the overall brightness
Sum variance [a]	Spread in the sum of the gray levels of voxel-pairs distribution
Sum entropy [a]	Randomness of the sum of gray levels of neighboring voxels
Histogram Features	Statistical values of the image intensities: Mean, Standard deviation, Kurtosis, Skewness, Maximum, Minimum, Median, Quartile, Range, and Entropy.

Texture features [a]; Gray-level co-occurrence matrix, GLCM.

Table 2 Patient femographics and characteristics of breast lesions

Characteristics	Total	Cross-validation Group			Test Group		
		Negative	Positive	*P*	Negative	Positive	*P*
	236	134	55		32	15	
Race							
African Amer	2	0	0	0.5582[a]	1	1	0.9698[a]
African American	31	19	12		0	0	
Asian	12	5	4		2	1	
Caucasian	176	107	39		21	9	
Hispanic	3	0	0		2	1	
Multiple Race	1	1	0		0	0	
Native Hawaiian	1	1	0		0	0	
Unknown	10	1	0		6	3	
Laterality							
Left	113	64	26	0.9513[b]	14	9	0.2989[b]
Right	123	70	29		18	6	
Age	47.9±9.0	47.8±8.8	48.9±8.6	0.4185[c]	47.9±10.1	45.3±8.7	0.4004[c]
Maximum Diameter[d]	4.47±1.91	4.46±1.88	4.51±2.01	0.8752[c]	4.11±1.80	5.14±1.86	0.0839[c]
Lesion Volume[e]	0.86±0.77	0.87±0.75	0.84±0.73	0.7970[c]	0.75±0.80	1.09±0.94	0.2122[c]
Parenchymal Density[f]	25.8±16.0	26.1±15.7	27.4±14.2	0.6216[c]	22.5±15.2	24.7±11.2	0.3914[c]

Fisher's exact test [a], χ^2 test [b], ANOVA [c], Centimeter [d], Cubic centimeter [e].

Proportion of parenchyma inside the breast [f], ±Standard deviation.

Table 3 Performance evaluation results of predictors formed by radiomic features

Region	Cross-validation Group				Test Group			
	Tumor		Parenchyma		Tumor		Parenchyma	
	AUC	*P*	AUC	*P*	AUC	*P*	AUC	*P*
undecomposed region	0.691 ± 0.072	\	0.589 ± 0.083	\	0.625 ± 0.056	\	0.524 ± 0.064	\
plasma-input	0.739 ± 0.070	0.2337	0.628 ± 0.072	0.7863	0.683 ± 0.044	0.7412	0.598 ± 0.041	0.5541
fast-flow	0.784 ± 0.062	0.0353	0.634 ± 0.082	0.5490	0.740 ± 0.061	0.1464	0.602 ± 0.062	0.4535
slow-flow	0.745 ± 0.065	0.1870	0.686 ± 0.075	0.0403	0.696 ± 0.052	0.5350	0.645 ± 0.058	0.1335
pure plasma-input	0.667 ± 0.078	0.2295	0.565 ± 0.081	0.2355	0.593 ± 0.035	0.8289	0.515 ± 0.034	0.9671
pure fast-flow	**0.816 ± 0.059**	**0.0128**	0.593 ± 0.079	0.8953	**0.785 ± 0.067**	**0.0389**	0.539 ± 0.051	0.8658
pure slow-flow	0.677 ± 0.075	0.7950	**0.702 ± 0.068**	**0.0204**	0.587 ± 0.059	0.6516	**0.681 ± 0.042**	**0.0407**
plasma ⋂ fast	0.732 ± 0.064	0.2830	0.549 ± 0.078	0.4180	0.671 ± 0.064	0.5646	0.509 ± 0.050	0.8278
plasma ⋂ slow	0.665 ± 0.073	0.3774	0.613 ± 0.074	0.8180	0.584 ± 0.060	0.6542	0.571 ± 0.038	0.7189
fast ⋂ slow	0.720 ± 0.066	0.3364	0.620 ± 0.069	0.7005	0.684 ± 0.058	0.5486	0.592 ± 0.056	0.6144
plasma ⋂ fast ⋂ slow	0.688 ± 0.073	0.9761	0.605 ± 0.076	0.9063	0.601 ± 0.047	0.9413	0.530 ± 0.047	0.9592

The values of AUC are presented along with 95% confidence intervals.

P for comparisons of prediction model performances.

Table 4 AUC comparison between CAM method and other methods (*P*)

Method	Cross-validation Group					Test Group				
	UTP	KPC	TTP	PER	CAM	UTP	KPC	TTP	PER	CAM
Tumor	0.7525↑	0.3230↑	0.0581↑	0.1845↑	0.0011↑	0.8696↑	0.4804↑	0.4045↑	0.4608↑	0.0397↑
UTS	—	0.5161↑	0.1410↑	0.3099↑	0.0099↑	—	0.6362↑	0.4812↑	0.4654↑	0.0450↑
KPC	—	—	0.4003↑	0.6969↑	0.0358↑	—	—	0.8366	0.9107↑	0.4598↑
TTP	—	—	—	0.6426↓	0.2082↑	—	—	—	0.9466↓	0.4011↑
PER	—	—	—	—	0.0951↑	—	—	—	—	0.2991↑

UTP, undecomposed tumor and parenchyma; KPC, kinetic pattern clustering; TTP, time to peak; PER, peak enhancement rate.

↑indicates that methods listed in the columns produce higher AUCs than those in the rows.

↓indicates that methods listed in the columns produce lower AUCs than those in the rows.

Figures

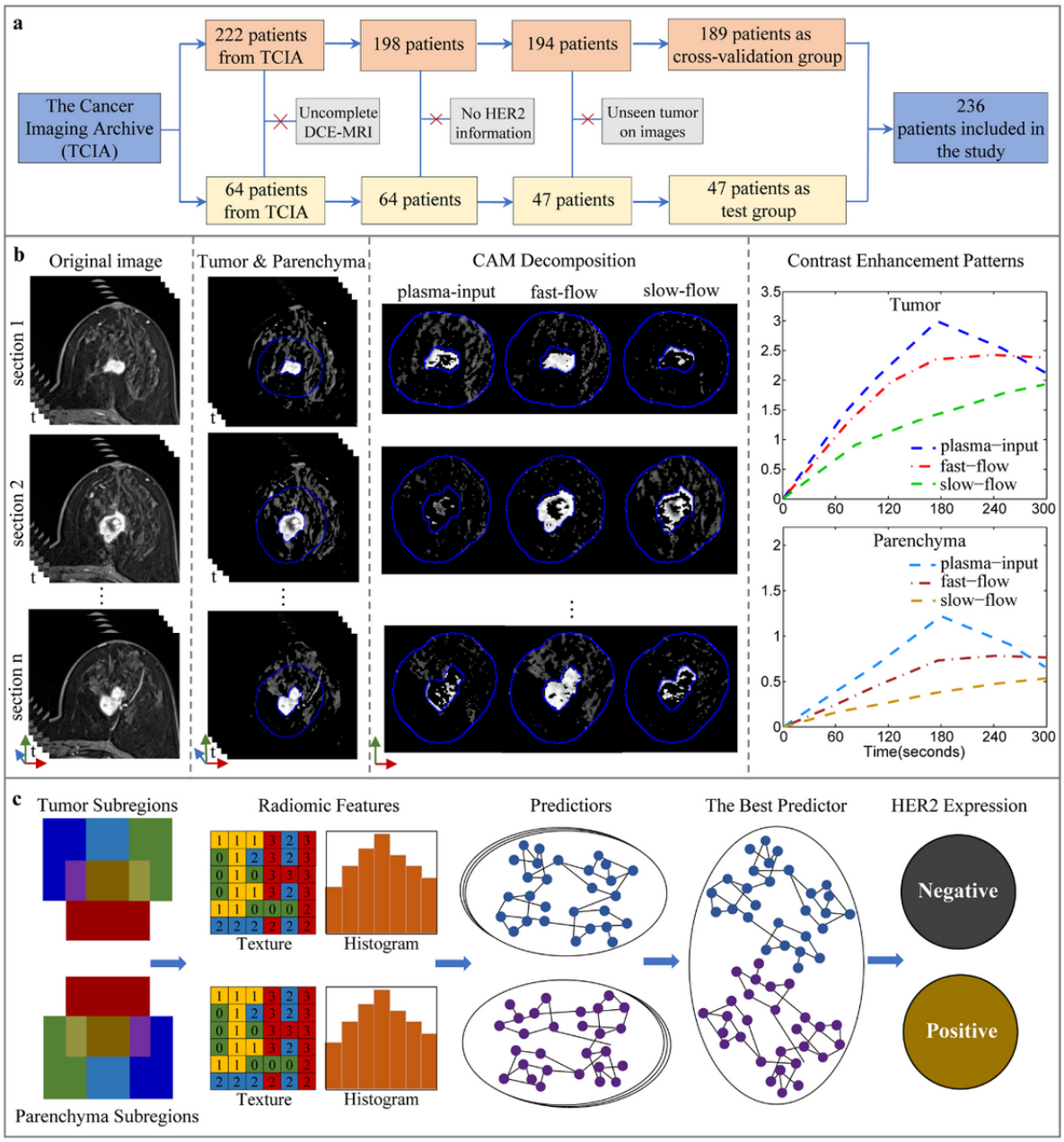

Figure 1

Flowchart of sample collection and the study. a. Inclusion and exclusion process of the study sample. b. Image processing, including segmentation of the tumor and its surrounding parenchyma, decomposition of DCE-MRI, observation of contrast enhancement patterns in subregions. c. Predictor building, including calculation of radiomic features, selection of predictive models, the fusion of predictive models.

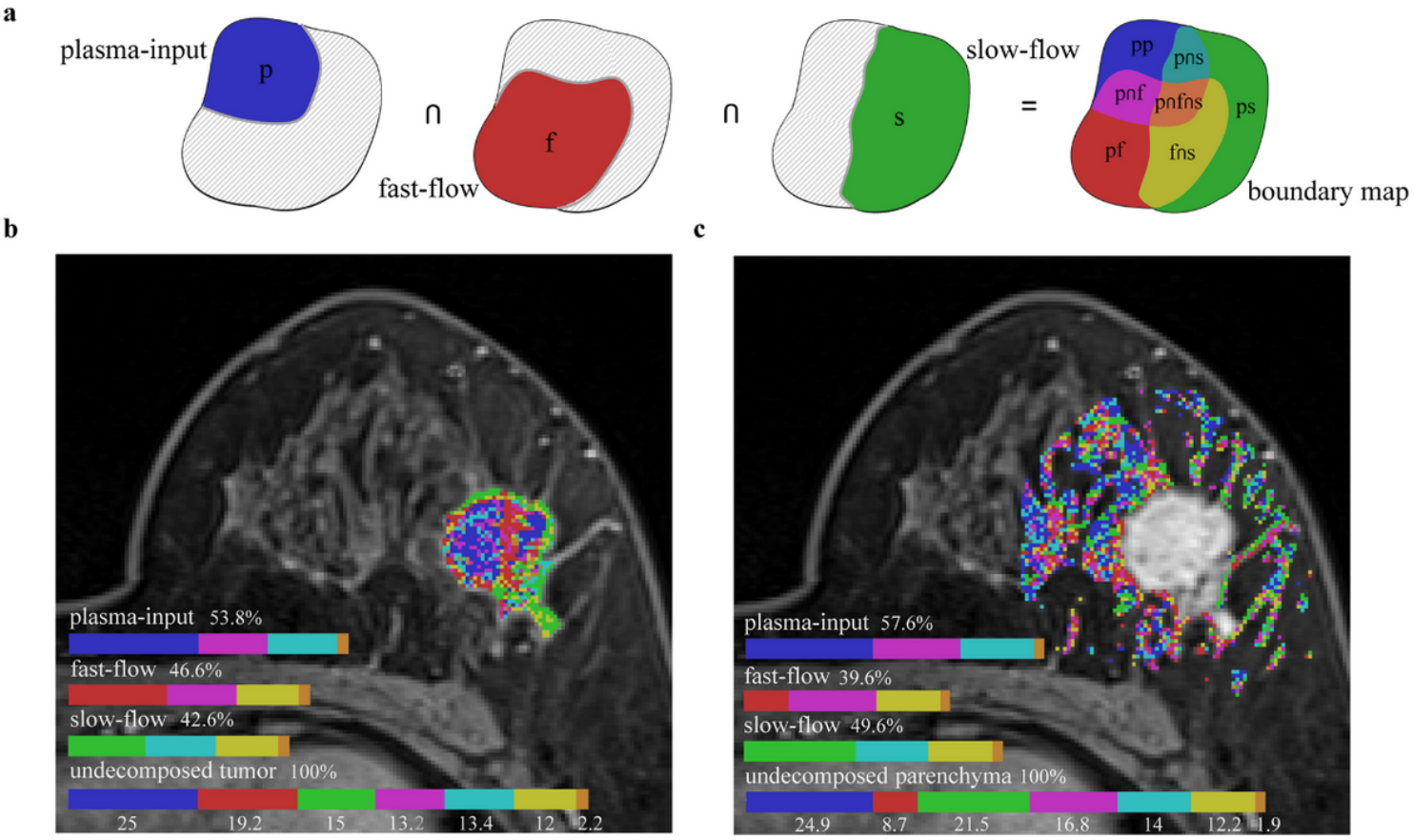

Figure 2

Tumor and parenchyma subregions decomposed by the convex analysis of mixtures (CAM) method. a. Schematic illustration of every subregion. p is plasma-input, f is fast-flow, s is slow-flow, pp is pure plasma-input, pf is pure fast-flow, ps is pure fast-flow, p∩f is plasma-input overlapped with fast-flow, p∩s is plasma-input overlapped with slow-flow, f∩s is fast-flow overlapped with slow-flow, p∩f∩s is plasma-input overlapped with flow-flow and slow-flow. b. The distribution map of subregions in a tumor of a breast cancer and percentages of every subregion. c. Corresponding information in the parenchyma.

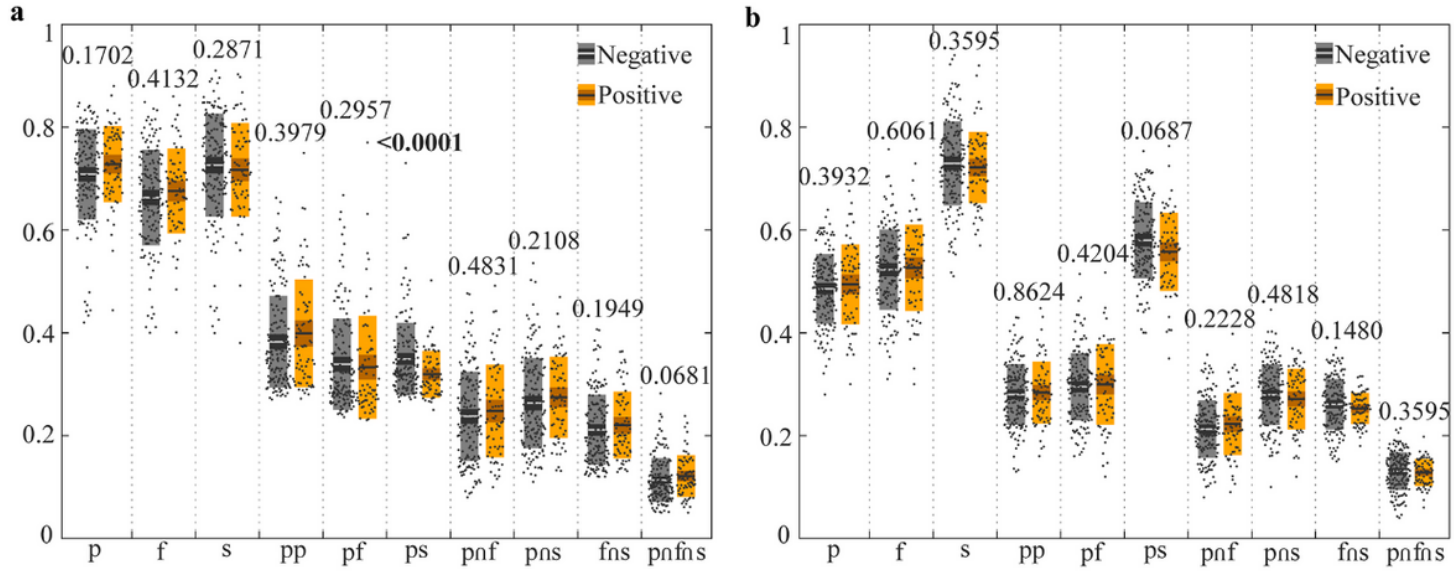

Figure 3

The area percentages of subregions in the undecomposed tissues. The Number at the top of the picture is P of ANOVA. a. Intratumoural corresponding information. b. Peritumoural corresponding information.

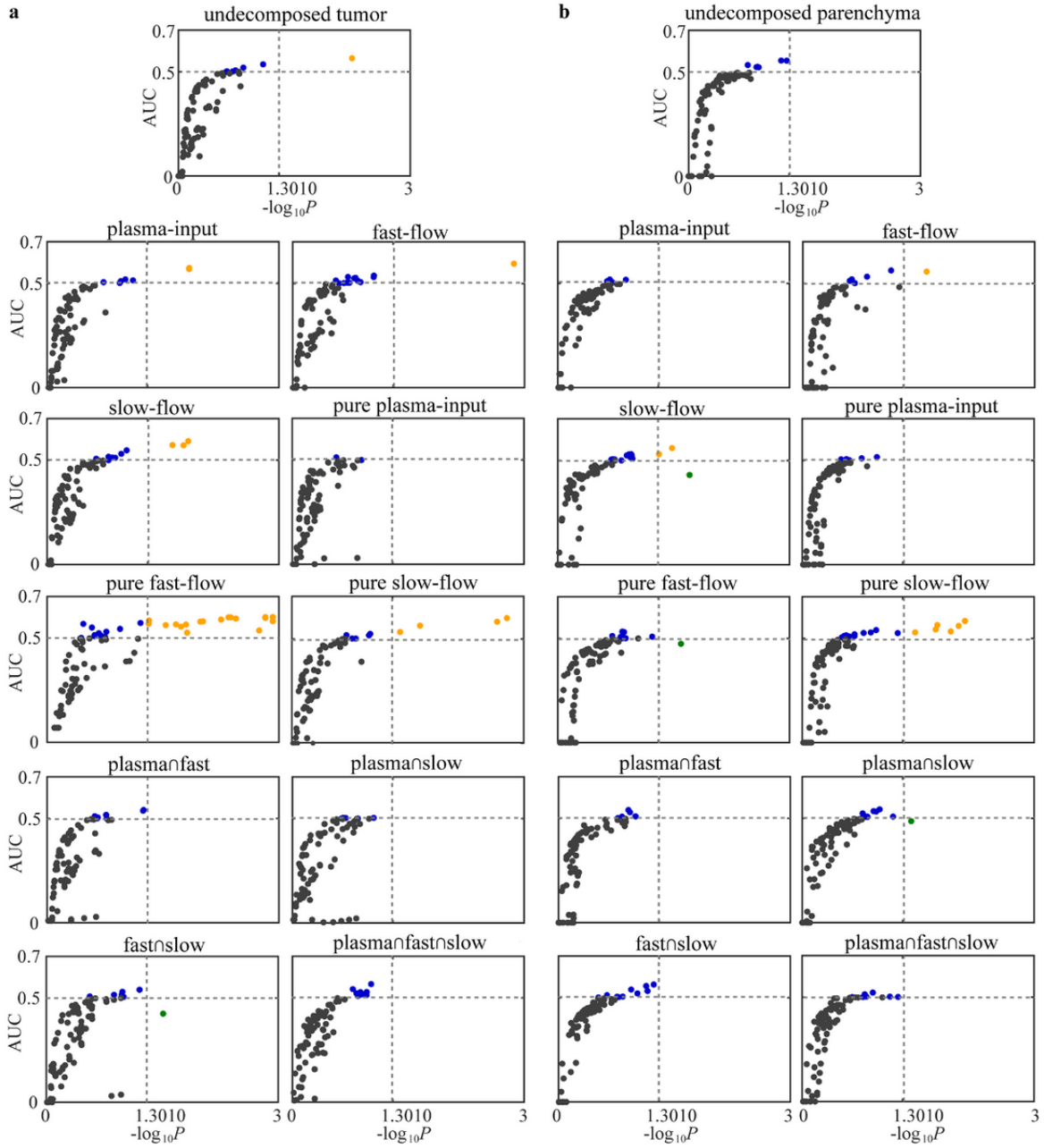

Figure 4

The chart of statistic differences and prediction performance of radiomic features in different regions. The abscissa is -log10P, and the ordinate is AUC. Yellow dots are P<0.05 and AUC>0.5, green dots are P <0.05 and AUC<0.5, blue dots are P>0.05 and AUC>0.5, black dots are P>0.05, and AUC<0.5. a. Tumor corresponding results. b. Parenchyma corresponding results

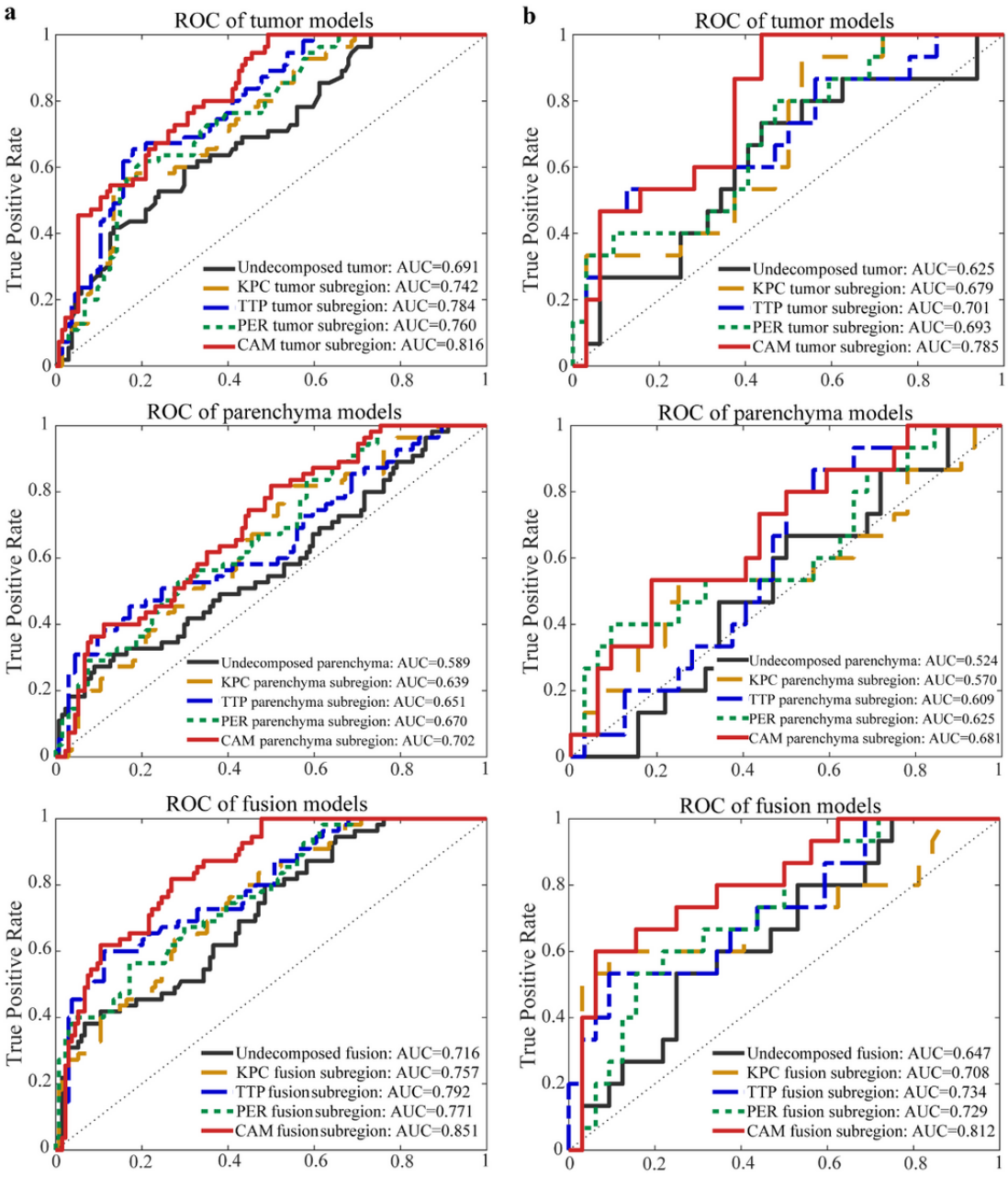

Figure 5

ROC plots of the prediction models of tumor, parenchyma, and fusion. Kinetic pattern clustering, KPC; time to peak, TTP; peak enhancement rate, PER; convex analysis of mixtures, CAM. a. ROC of cross-validation group. b. ROC of the test group.